Journal of Applied Polymer Science

Size-controlled gold nanoparticles inside polyacrylamide microgels

M. Díaz,[1] A. Barrera,[2] S. López-Cuenca,[3] S. Y. Martínez-Salazar,[2] M. Rabelero,[4] I. Ceja,[5] V. V. A. Fernández,[1] J. Aguilar[1]

[1]Departamento de Ciencias Tecnológicas, Universidad de Guadalajara, Avenida Universidad 1115, 47820, Ocotlán Jalisco 47820, Mexico

[2]Departamento de Ciencias Básicas, Universidad de Guadalajara, Avenida Universidad 1115, 47820 Ocotlán Jalisco 47820, Mexico

[3]Instituto Tecnológico Superior de Tequila, Joel Magallanes Rubio 501, Col. Lomas del Paraíso 46400 Tequila Jalisco, Mexico

[4]Departamento de Ingeniería Química, Universidad de Guadalajara, Boulevard M. García Barragán 1451, 44430 Guadalajara Jalisco, Mexico

[5]Departamento de Física, Universidad de Guadalajara, Boulevard M. García Barragán 1451, 44430 Guadalajara Jalisco, Mexico

Correspondence to: J. Aguilar (E-mail: jacob161111@gmail.com)

ABSTRACT: Gold nanoparticles (AuNPs) of different sizes were synthesized into a crosslinked network of polyacrylamide (PAAm) microgels. PAAm was prepared by means of semicontinuous inverse heterophase polymerization under monomer-starving conditions with a *z*-average particle size of 384 ± 18 nm. AuNPs with controlled size were obtained by a reduction reaction of Au^{+3} to Au^0 from a gold(III) chloride trihydrate ($HAuCl_4$) solution inside microgel the crosslinked network (AuNP-PAAm). The reduction reaction was verified for 2 h by ultraviolet–visible spectroscopy (UV–vis). AuNP–PAAm exhibited a particle size between 288 ± 12 and 230 ± 15 nm at $HAuCl_4$ concentrations of 0.4 and 1.3 m*M*, respectively. The AuNP–PAAms were observed by transmission electron microscopy, and their sizes were determined to be 19 ± 2 nm (1.3 m*M*) and 17 ± 2 nm (1.1 m*M*). With UV–vis spectroscopy, we detected the formation of AuNPs at a wavelength of 552 nm, and with X-ray diffraction analysis, we proved that the crystal arrangement was face-centered cubic. © 2016 Wiley Periodicals, Inc. J. Appl. Polym. Sci. **2016**, *133*, 43560.

KEYWORDS: crosslinking; microgels; morphology; nanoparticles; nanowires; nanocrystals; swelling

Received 15 August 2015; accepted 18 February 2016

DOI: 10.1002/app.43560

INTRODUCTION

The physical and chemical properties of many materials depend on their particle sizes. When the size can be controlled, innovative and compelling applications can be obtained. Many applications have been found in different areas, including particle size in catalysis,[1–7] chemical separations,[8] sensors,[9–11] medical applications,[12–15] and electrical conductivity.[16]

There are several methods for synthesizing gold nanoparticles (AuNPs) with reducing agents. A common method is the use of solvable surfactants, that is, cetyltrimethylammonium salts, and sodium bis(2-ethylhexyl) sulfosuccinate in water to form micelles.[17–20] Another method is the Turkevich method, which uses sodium citrate as a reducing agent at a high pH and temperature in a gold(III) chloride trihydrate ($HAuCl_4$) solution, where the nanoparticle size depends on the citrate/$HAuCl_4$ relationship.[21–24] Brust *et al.*[25] synthesized thiol-derivatized AuNPs in a two-phase liquid–liquid system, where the particles were grown in two-phases; this allowed a surface reaction to take place during metal nucleation and growth. Amine groups possess high potential for metal reduction and oxidation. Newman and Blanchard[26] used amines as reducing agents for the formation of AuNPs. Kumar *et al.*[27] investigated the interaction between surface-bonded alkyl amines and AuNPs. They reported two different ways of binding the amine molecules to the AuNPs: (1) a weakly electrostatic complex bonding involving protonated amine molecules and (2) AuNP interaction with surface-bound chloroaurate ions, where $AuCl(NH_2R)$ complexes presented strong bonds. Several methods for the *in situ* synthesis of metal nanoparticles (i.e., Au, Cu, Co, Pt, Ni, and Ru) with hydrogels as a polymeric network template in several forms, such as bulk gels, cryogels, and microgels, have recently been reported.[28–30] Some authors synthesized AuNPs through the reduction of $HAuCl_4$ with core–shell microgels of

Additional Supporting Information may be found in the online version of this article

poly(*N*-isopropyl acrylamide)/polyethyleneimine[31] and poly(*N*-isopropyl acrylamide)/polystyrene.[32] Others reported the synthesis of yolk–shell poly(*N*-isopropyl acrylamide) particles.[33] The incorporation of metal nanoparticles into the network microgel improves its mechanical properties[34] and can also impart electrical,[35] magnetic,[36,37] and catalytic[30] features to the microgels. Zhang and Kumacheva[38] used poly(acrylic acid) microgels for the synthesis of semiconductor, metal, and magnetic nanoparticles.

There are many variables that affect the control of the AuNP size and distribution; these include the substance-to-molar ratio of the reducing agent, the stabilizing agent, and the reaction time and temperature.[39] Such variables can be controlled during AuNP preparation, where chemical reduction is performed with a gold acid aqueous solution. Moreover, gold-colored nanoparticles also depend on the shape and size and the dielectric constant of the solvent used.[40] The synthesis of monodisperse AuNPs is also mainly controlled by the number of produced nucleating centers in size-controlled polymeric network templates. Thus, efforts have been made to obtain microgels with controlled sizes, porosity, and morphology.[41]

Recently, we reported the synthesis of poly(*N*-isopropyl acrylamide) nanogels with controlled sizes (39–46 nm) and narrow distributions (~1.3) by a semicontinuous inverse heterophase polymerization (SIHP) process under monomer-starving conditions. A low weight ratio of 0.3 of the polymer produced to the surfactant used was obtained.[42] The SIHP process under monomer-starving conditions was achieved to obtain specific characteristics of polymers, such as a controlled average molecular weight and a low particle size with a narrow distribution and high solids content.[43] SIHP under monomer-starving conditions consists of an aqueous solution of a monomer that is fed continuously at a controlled rate into a monomer-free surfactant-and-initiator oleic solution to minimize the formation of emulsified monomer droplets and to achieve monomer-starved conditions.

In this study, we report the *in situ* synthesis of AuNPs with different controlled sizes, from polyacrylamide (PAAm) spherical microgel networks prepared by SIHP with different concentrations of $HAuCl_4$ without the presence of any reducing agent at 25 °C. We found that the gold particle size was dependent only on the $HAuCl_4$ concentration when the initial microgel size was practically constant with narrow distributions.

EXPERIMENTAL

The chemicals reagents and solvents used were as follows: acrylamide (AA; Sigma, 99% pure), sodium bis(2-ethylhexyl) sulfosuccinate (Sigma, 96% pure), *N,N′*-methylene bisacrylamide (Sigma, 99% pure), benzoyl peroxide (Sigma, 75% pure), toluene (Sigma, 95% pure), $HAuCl_4 \cdot 3H_2O$ (Sigma, 95% pure), and bidistilled and deionized water.

The synthesis of AuNP–PAAm was performed with a two-stage synthesis process. First, spherical microgels of PAAm were prepared by SIHP under monomer-starving conditions. A 250-mL reactor was initially charged with a solution of sodium bis(2-ethylhexyl) sulfosuccinate/toluene at a weight ratio of 0.25 g/g; this was heated at 50 °C under an argon atmosphere and allowed to stabilize. A small quantity of toluene was used to prepare a solution containing benzoyl peroxide (1 wt % with respect to AA); this was added to the main solution, with a total mass of 85.5 g, under continuous agitation for 30 min. Otherwise, an aqueous solution of AA (AA/water w/w = 0.9 g/g) and 1 wt % *N,N′*-methylene bisacrylamide (on the basis of AA) was added to the reactor at a 0.2 g/min feeding rate with a dosing syringe pump (Kd Scientific 200 series) to start the polymerization reaction. The full feeding time was 73 min. The reaction was allowed to proceed for an additional 2 h to allow it to reach maximum conversion. For the second synthesis stage, the microgels synthesized in the first stage were deposited inside a Millipore membrane (molecular weight cutoff = 6000–8000) and immersed in bidistilled water to remove the surfactant and residual initiator until the ionic conductivity was less than 6 μS/cm. After this, the purified microgels were dried in an oven at 40 °C for 24 h. Samples weighing 0.04 g of the dried microgels were deposited into vials containing 4 g of different concentrations of $HAuCl_4$ aqueous solutions (0, 0.4, 0.7, 0.9, 1.1, and 1.3 m*M*). These dispersions were placed inside an ultrasonic cleaner apparatus, where the reduction reaction took place for 2 h at 25 °C (Figure S1, Supporting Information).

The *z*-average particle sizes (Dp_z) of the microgels were measured at 25 °C by dynamic light scattering (DLS) in a Malvern Zetasizer ZS90 apparatus. The standard operating procedure subroutine of the DLS instrument automatically calculated the particle distribution. The swelling kinetics determination of the microgels was followed by DLS, where each measurement was obtained at intervals of 8 min.

AuNP–PAAm was observed in a JEOL 1010 transmission electron microscope at an accelerating voltage of 100 kV to measure the PAAm and AuNP–PAAm particle size and the shape of the dried microgels. A drop of the withdrawn sample of each microgel was deposited onto a carbon-coated copper grid afterward in a vacuum oven at 50 °C for 12 h before it was observed with a microscope.

Raman spectra were obtained with a Raman Thermo-Nicolet apparatus (Almega model) equipped with a diode-pumped in solid state of Nd:YVO_4 as laser source to detect the presence of AuNPs inside the microgels. The laser excitation line was 532 nm, and the laser power was 25 mW. Raman spectra were recorded in a 300–1800-cm^{-1} range, where the resolution was limited to 1 cm^{-1} with 25 s of integration time. The PAAm and AuNP–PAAm dispersions were deposited inside an optical glass cell when the measurements were performed.

X-ray diffraction (XRD) analysis was performed in a θ–θ diffractometer system (θ is the scatering angle) from Stadip (STOE & Cie GmbH, Darmstadt, Germany) equipped with a copper source operated at 30 kV and 15 mA, with a Kα radiation of 1.5406 Å over a scattering angle (2θ) range of 5–80° to determine the AuNP arrangement inside the microgels. Dried samples were ground into a fine powder and then fixed on a glass slide with Vaseline, which did not interfere with the sample measurement.

UV–vis spectra were recorded in a 400–800-nm wavelength range with a Varian (Cary-300) spectrometer. Samples of the

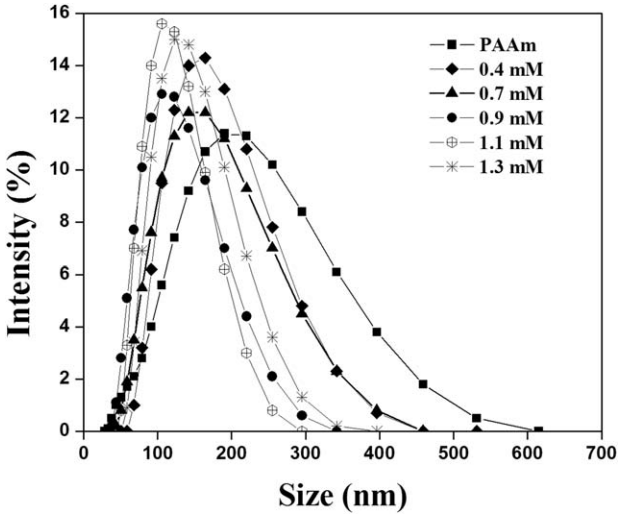

Figure 1. Intensity size distribution measured by DLS at 25 °C for PAAm and AuNP–PAAm.

AuNP–PAAm dispersions were withdrawn at given times to measure the AuNP formation kinetics.

Open-circuit potential (OCP) measurements were conducted to follow the reduction kinetics inside the microgels. OCP measurements were performed with an Autolab PGSTAT 128N potentiostat controlled by the commercial Nova 1.10 software. A standard three-electrode cell from Fisher Scientific was used to obtain the measurements. The working electrode was a gold disc electrode with a diameter of 1.6 mm embedded in Teflon. The auxiliary electrode was a long Pt wire, and the reference was a saturated calomel electrode (SCE). We prepared the working solution by weighing 4 g of a 1.1 m*M* aqueous solution of $HAuCl_4$. The gold solution was mixed with 0.04 g of the dried microgels and placed in a forced recirculation bath at 25 °C with a digital temperature control to obtain the reaction reduction kinetics.

AuNPs were observed with field emission scanning electron microscopy (FESEM) with a TESCAN model MIRA operated at 20 KeV. An energy-dispersive X-ray spectroscope from Bruker (model XFlash 6130) was used at a 15-beam intensity to analyze the gold composition in the FESEM image from the sample.

RESULTS AND DISCUSSION

Figure 1 depicts the particle size distributions obtained from PAAm and AuNP–PAAm at different $HAuCl_4$ concentrations, as measured by DLS at 25 °C. Table I reports Dp_z and the polydispersity index. Figure 1 shows that the PAAm particle size was higher and the distribution was broader than those of AuNP–PAAm. In fact, the size of the PAAm was practically constant (384 ± 18 nm) and was maintained with the SIHP process, whereas the AuNP–PAAm size decreased as the $HAuCl_4$ concentration increased (Table I). PAAm had hydrogen atoms and carbonyl free groups, which interacted with water molecules, increasing the swelling of the PAAm microgels. When the $HAuCl_4$ concentration increased, the AuNP size also increased, and therefore, the size of AuNP–PAAm decreased, and its distributions tended to be narrower. We propose that the AuNPs inside the microgels limited the interaction of the hydrogen and oxygen bonds of water molecules with amide groups; this reduced the swelling of PAAm. Therefore, as the AuNP size increased, the mesh of the crosslinked network began to become saturated; this prevented more water molecules from interacting with amine groups and decreased the particle sizes of the microgels. It is well known that amine groups act as a reductant in $HAuCl_4$ solutions.[26,27,44] However, with amide groups, it is more difficult to reduce the gold from $HAuCl_4$ because it is not protonated; hence, the gold reduction in this process could be performed by the protonating nitrogen atom when the amide was destabilized by the presence of aqueous $HAuCl_4$.

Figure 2(a,b) shows the transmission electron microscopy (TEM) micrographs of the AuNPs in which quasi-spherical nanoparticles were observed with average diameters of about 17 ± 1 and 19 ± 2 nm for $HAuCl_4$ concentrations of 1.1 and 1.3 m*M*, respectively. Table I reports the average size of the AuNPs for all of the $HAuCl_4$ concentrations. The dried PAAm structure (without AuNPs) was observed by TEM to determine Dp_z and shape of the dry microgels. Figure S2 (Supporting Information) shows the TEM micrographs of PAAm that disclose quasi-spherical particles with a Dp_z of 102 ± 11 nm. Some of the microgels had a porous structure.

The presence of AuNPs inside the PAAm microgels was confirmed by FESEM. Figure 2(c) shows dry microgels with AuNPs within its structure, where their Dp_z was 97 nm at a concentration of 1.1 m*M*. Analysis performed by energy-dispersive X-ray spectroscopy [Figure 2(d)] was used to confirm the presence of AuNPs; it was detected the Au element at about 2 and 9.5 KeV. This result supported the formation of AuNPs inside the internal structure of the microgel. Moreover, peaks of the C, N, Cu, Ti, and O elements appear in Figure 2(d), and elements such as Cu and Ti were derived from the copper grid and the sputtering target, respectively.

UV–vis spectra of AuNP–PAAm synthesized at different concentrations of $HAuCl_4$ are illustrated in Figure 3. This technique allowed us to monitor the synthesis of AuNPs localized inside

Table I. Dp_z values of PAAm, AuNP–PAAm from different concentrations (mM) of $HAuCl_4$ and their Distribution (Polydispersity Index) from DLS, AuNP average sizes from the TEM and XRD Spectra

Sample	Dp_z (nm)[a]	Polydispersity index[a]	Average AuNP size[b]	AuNP average size (L)[c]
PAAm	384 ± 18	1.6	—	—
0.4 m*M*	288 ± 12	1.4	10 ± 1	—
0.7 m*M*	294 ± 14	1.5	12 ± 1	—
0.9 m*M*	214 ± 9	1.5	15 ± 1	16
1.1 m*M*	207 ± 14	1.4	17 ± 1	18
1.3 m*M*	230 ± 15	1.4	19 ± 2	21

[a] Determined by DLS.
[b] Determined from 50 AuNP measurements of the TEM photographs.
[c] Calculated by Debye-Scherrer equation from XRD data.

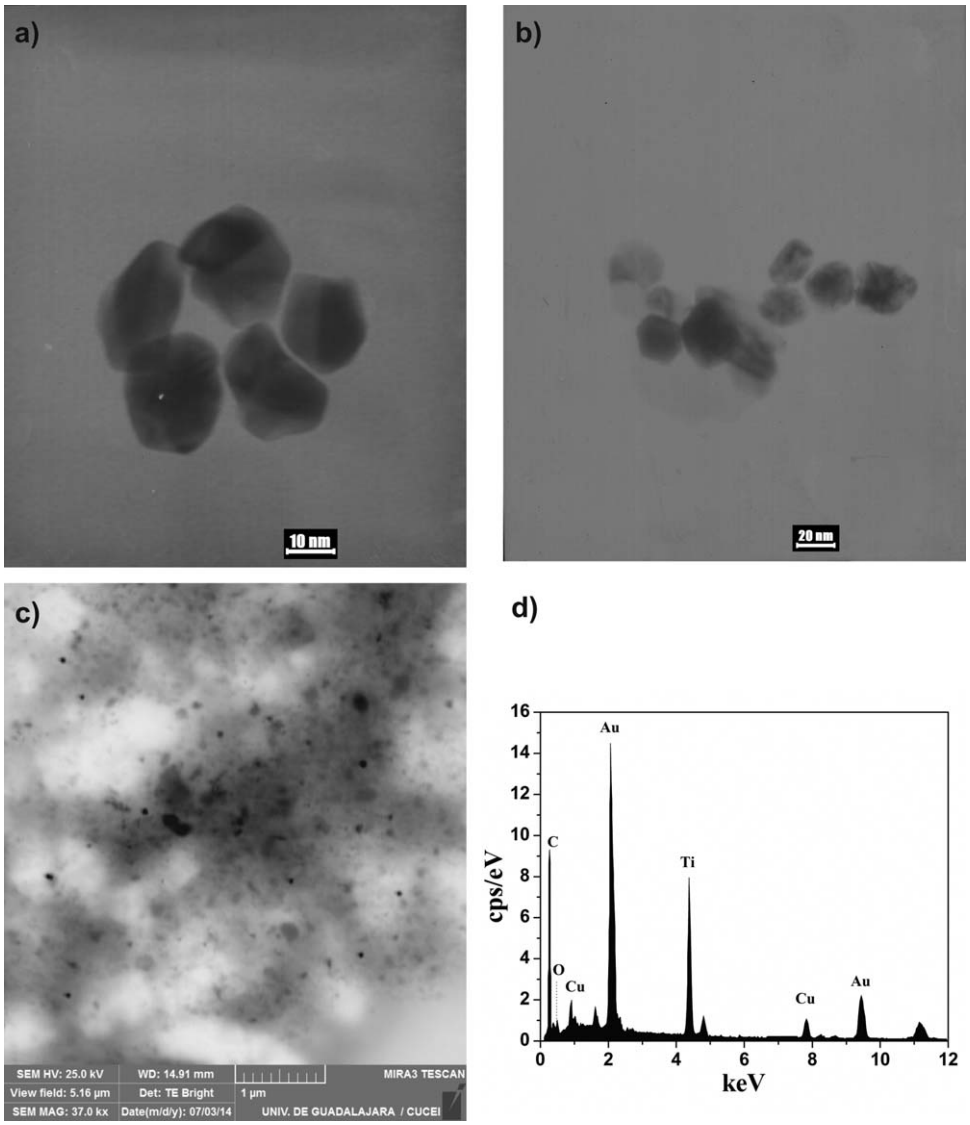

Figure 2. TEM micrographs of the AuNPs: (a) 1.1 m*M* $HAuCl_4$ and (b) 1.3 m*M* $HAuCl_4$. (c) Scanning electron microscopy micrograph of AuNP–PAAm at an $HAuCl_4$ concentration of 1.1 m*M*. (d) Energy-dispersive X-ray spectroscopy spectrum from panel c; counts per second (cps).

the microgels on the basis of their surface plasmon resonance (SPR). The absorption band observed of an SPR for 0.4 m*M* was at 526 nm. As the concentration of $HAuCl_4$ increased, the absorption band became more intense and shifted to longer wavelengths of up to 540 nm for the 1.3 m*M* concentration. Gold-colored nanoparticles appeared and changed coloration with an increase in the concentration. For smaller concentrations, the nanoparticle color was pinkish red. For medium concentrations, the color was purple, and at higher concentrations, the color tended to be brownish red (Figure S3, Supporting Information).

The reaction kinetics were followed by UV–vis spectroscopy for a 1.3 m*M* concentration. As the time increased, the maximum peak was obtained at about 2 h under continuous sonication. The measurements were each taken at 12-min intervals. SPR remained at the same wavelength throughout the reduction reaction. This demonstrated that the AuNPs were dispersed homogeneously inside the microgel; therefore, this suggested

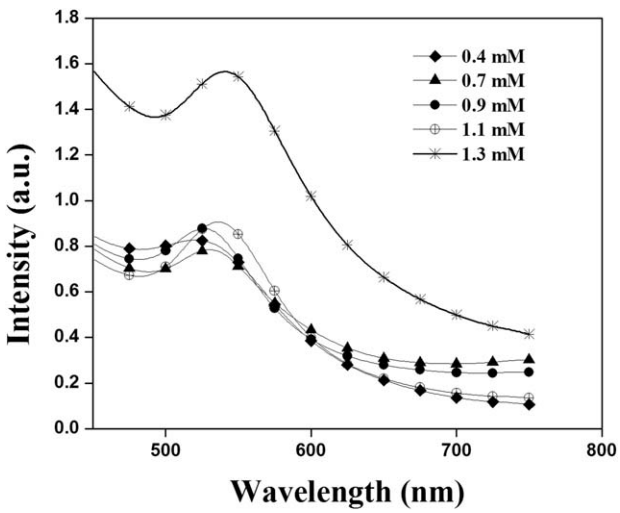

Figure 3. UV–vis spectra of AuNP–PAAm.

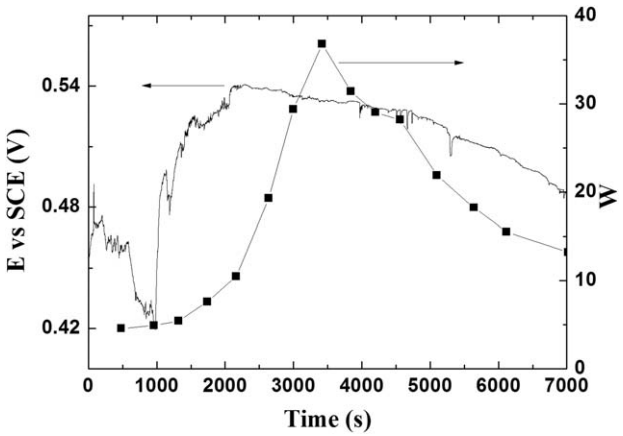

Figure 4. (—) OCP versus time for PAAm in a 1.1 m*M* $HAuCl_4$ solution with sonication. (■) Swelling kinetics (W) of PAAm in a 1.1 m*M* $HAuCl_4$ solution.

that there was no aggregation of the nanoparticles (Figure S4, Supporting Information).

Figure 4 shows the plots of evolution of the OCP (E vs SCE (V), where E, is electrode potential) in which the current flowing at the gold electrode and the solution of $HAuCl_4$ (in the presence of the microgels) interface was zero and the PAAm swelling kinetics [aqueous $HAuCl_4$ solution uptake (W) vs time]. A slow variation in the potential at short times was observed. However, a significant increment in OCP was observed when the time increased until it reached almost a constant value. The increment in OCP at long times suggested that more energy was required to reach a zero current value, and as a consequence, a thermodynamic equilibrium between the work electrode and the ions was present in the solution. We related this behavior to the reduction of Au^{+3} produced by the presence of the amide. As the time increased, less Au^{+3} was present in the solution, and more Au^0 was formed in the microgel. Thus, the thermodynamic equilibrium was reached at more positive OCP values.

On the other hand, for the swelling behavior of PAAm, W was obtained from[42]

$$W = \frac{V(t) - V_{dry}}{V_{dry}} \quad (1)$$

where $V(t)$ is the volume of the swollen PAAm at a given time (t) calculated from the DLS-measured size (Dp_z) and V_{dry} is the volume of the dry PAAm estimated by the measurement of its dry diameter (d_0) from the TEM micrograph (Figure S2, Supporting Information). d_0 is related to the volume swelling ratio as follows[45]:

$$\frac{\phi_0}{\phi} = \left(\frac{d}{d_0}\right)^3 \quad (2)$$

where ϕ and ϕ_0 are the network volume fractions at swelling equilibrium and the reference state, respectively, and d is the swollen PAAm diameter (Dp_z) measured by DLS.

Figure 4 shows that PAAm swelled fast, whereas W increased with time up to a maximum swelling value (W_{max}) of 36.8. It was not possible to observe the equilibrium W in the range of time analyzed. On the other hand, W presented a similar behavior to the OCP curves. At $t > W_{max}$, W decreased; this indicated that the PAAm deswelled in the presence of AuNPs, which displaced the water molecules outside of the microgels in a manner similar to a particle close-packing phenomena. These results suggest that the reduction reaction of Au^{+3} to Au^0 was carried out inside the PAAm. However, it was important that the gold reduction was also achieved outside the microgels.

Raman measurements were performed for PAAm and AuNP–PAAm at different $HAuCl_4$ concentrations (Figure 5). The Raman spectra of PAAm has been widely studied.[46–48] The PAAm and AuNP–PAAm spectra were analyzed from 300 to 1800 cm^{-1}, and the different absorption bands were correlated: at 1106 cm^{-1}. A midband appeared because of CH bending (δCH), strong bands due to CH_2 bending (δCH_2) appeared at 1328 cm^{-1}, and CH_2 symmetric stretching (v_sCH_2) at 1495 cm^{-1} caused by C—C symmetric stretching was observed. The remaining strong band localized at 1260 cm^{-1} was due to CH_2 asymmetric stretching (v_aCH_2); the band at 1392 cm^{-1} was due to strong vibrations of C—N bonds, and the band at 1202 cm^{-1} was due to NH_2 wagging (γNH_2). In the PAAm and AuNP–PAAm spectra at concentrations of 0.4 and 0.7 m*M*, respectively, we observed a midband at 1202 cm^{-1}; however, this band disappeared at higher concentrations of 0.7 m*M*. This indicated that there was a chemical interaction with $AuCl_4^-$ ions with the amide groups. Such interactions could be demonstrated in the absence of γNH_2 bands.

The X-ray diffraction patterns of AuNP–PAAm at the different $HAuCl_4$ concentrations (0.4, 0.7, 0.9, 1.1, and 1.3 m*M*) are presented in Figure 6. For the 0.4 and 0.7 m*M* concentrations, it was not possible to observe the characteristic peaks of gold when the crystalline arrangement was not yet fully formed or

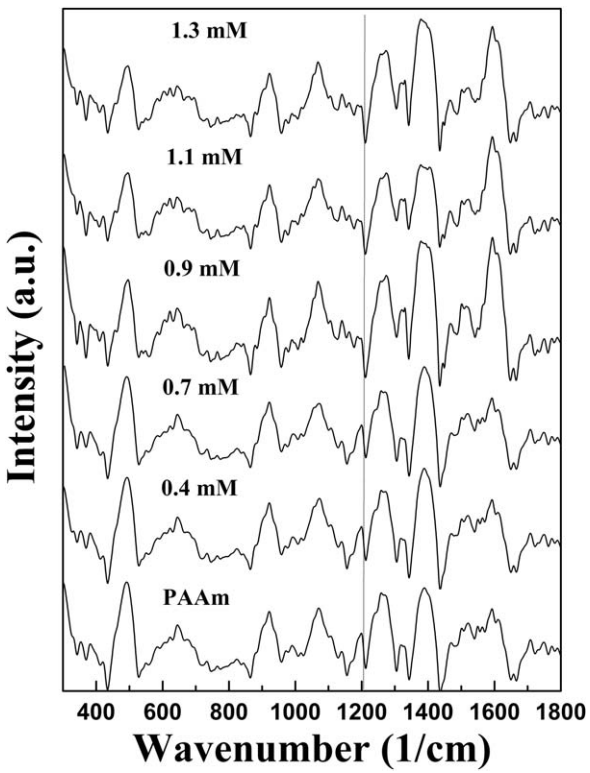

Figure 5. Raman spectra of PAAm and AuNP–PAAm.

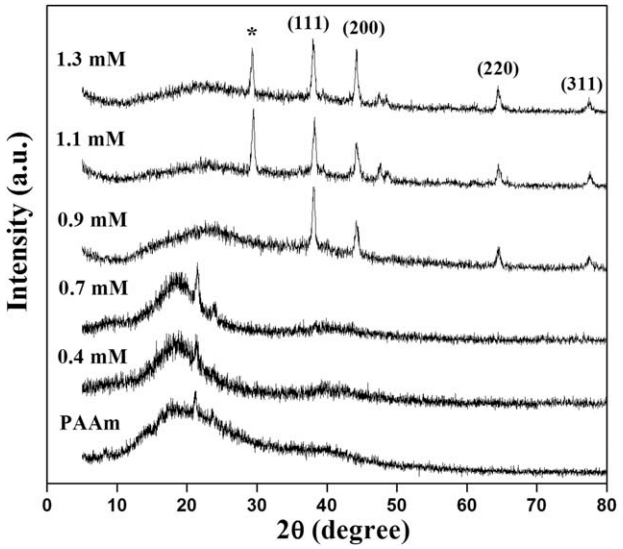

Figure 6. XRD patterns of AuNP–PAAm.

the crystal size was very small. The two peaks appearing at 2θ angles around 22 and 24° corresponded to reflections of the sample holder. At concentrations above 0.7 m*M*, the diffraction peaks were well defined, and the four characteristic AuNP diffraction peaks appeared. These peaks were localized at 2θ angles of 38.1, 44.3, 64.5, and 77.6° and were related to the crystalline planes (111), (200), (220), and (311), respectively, of the AuNPs.[2,49] The broad peak observed in the 2θ angle range between 12 and 27° was attributed to PAAm.[49–51] In the XRD patterns of AuNP–PAAm for $HAuCl_4$ concentrations higher than 1.1 m*M*, there was an unidentified diffraction peak (*) at about $2\theta = 29°$: we propose that the AuNP–$AuCl_4^-$ crystals interacted with the amide groups of PAAm, as shown in the Raman spectroscopy studies; this could have generated a new phase that was not identified in this study. According to the Joint Committee Powder Diffraction Standards data card No. 4-784, the AuNPs presented a face-centered cubic arrangement.

The average size of crystalline domains (L) of the AuNPs was calculated by the Debye–Scherrer equation from the XRD data (Figure 6) as follows[52]:

$$L = \frac{k\lambda}{\beta\cos\theta} \tag{3}$$

where $k = 0.9$ is the Debye–Scherrer constant related to the crystalline structure, λ is the wavelength (nm), and β is the line widening at the half-maximum peak (2θ; rad) and denominated as the full width at half-maximum. Calculations were performed with the assumption of Gaussian behavior. The average size value obtained by both techniques was very close for each concentration. However, the sizes of the 0.4 and 0.7 m*M* concentrations were lower; thus, it was not possible to calculate them from the XRD measurements because the peaks in these diffractograms were not well defined (Table I).

CONCLUSIONS

In this article, we have reported the synthesis of AuNPs with PAAm microgels as a reductant. By means of the SIHP process, it was possible to synthesize PAAm microgels with a controlled size distribution and particle size. Such factors are important because they allowed us to obtain a controlled mesh size with improved homogeneous $HAuCl_4$ distribution into the microgel while preventing AuNP agglomeration. Consequently, this afforded us better control of the AuNP size. Also, increasing the contact area between the $HAuCl_4$ solution and the microgels increased the reduction reaction rate. Moreover, we studied several concentrations of $HAuCl_4$, and as a result, reductions were obtained of nanoparticles of different sizes; this will expand their applications, such as in catalysts or medical applications, such as chemotherapy and the diagnosis of cancer cells. This technique is becoming important because it is not necessary to use a catalyst, initiator, stabilizer, or any reductant agent because PAAm acts as these. From UV–vis spectroscopy, we demonstrated the formation of AuNPs, which were absorbed in the visible spectrum; this feature will allow us to use them as catalysts or photovoltaic cells in specific matrices. The Raman technique permitted us to identify the chemical interaction of AuNPs with the microgels, which could maintain the nanoparticle stability for a long time. Finally, we observed by XRD that the intensity of the characteristic peaks increased; this demonstrated that there was an increase in the AuNP size as the $HAuCl_4$ concentration increased.

ACKNOWLEDGMENTS

One of the authors (M.D.) acknowledges a scholarship from Consejo Nacional de Ciencia y Tecnología.

REFERENCES

1. Haruta, M.; Yamada, N.; Kobayashi, T.; Lijima, T. J. *Catal.* **1989**, *115*, 301.
2. Panigrahi, S.; Basu, S.; Praharaj, S.; Pande, S.; Jana, S.; Pal, A.; Kumar, S.; Pal, T. *J. Phys. Chem. C* **2007**, *111*, 4596.
3. Stratakis, M.; García, H. *Chem. Rev.* **2012**, *112*, 4469.
4. Theodoros, S.; Loannis, L.; Konstantinos, L. *Tetrahedron* **2013**, *69*, 4612.
5. Petros, G.; Manolis, S.; Loannis, L. *Catal. Commun.* **2013**, *36*, 48.
6. Ramírez, J.; Sanaú, M.; Fernández, E. *Angew. Chem. Int. Ed.* **2008**, *120*, 5272.
7. Shanahan, A. E.; Sullivan, J. A.; McNamara, M.; Byrne, H. J. *New Carbon Mater.* **2011**, *26*, 347.
8. Gross, G. M.; Nelson, D. A.; Grate, J. W.; Synovec, R. *E. Anal. Chem.* **2003**, *75*, 4558.
9. Guidelli, E. J.; Ramos, A. P.; Zaniquelli, M. E. D.; Nicolucci, P.; Baffa, O. *ACS Appl. Mater. Interfaces* **2012**, *4*, 5844.
10. Chen, L.; Lu, W.; Wang, X.; Chen, L. *Sens. Actuators B* **2013**, *182*, 482.
11. Mingjian, Y.; Yongjun, L. I.; Huibiao, L. I. U.; Yuliang, L. I. *Sci. China Ser. B* **2009**, *52*, 715.
12. Thakor, A. S.; Jokerst, J.; Zavaleta, C.; Massoud, T. F.; Gambhir, S. S. *Nano Lett.* **2011**, *11*, 4029.

13. Hayashi, A.; Naseri, A.; Pennesi, M. E.; de Juan, E., Jr. *Jpn. J. Ophthalmol.* **2009**, *53*, 249.
14. Krpetic, Z.; Porta, F.; Scarì, G. *Gold Bull.* **2006**, *39*, 66.
15. Yun, G. E.; Bin, K. *Sci. China Ser. E* **2011**, *54*, 2358.
16. Jana, S.; Salehi-Khojin, A.; Zhong, W. H.; Chen, H.; Liu, X.; Huo, Q. *Solid State Ionics* **2007**, *178*, 1180.
17. Kawasaki, H.; Nishimura, K.; Arakawa, R. *J. Phys. Chem. C* **2007**, *111*, 2683.
18. Prasad, B. L. V.; Arumugam, S. K.; Bala, T.; Sastry, M. *Langmuir* **2005**, *21*, 822.
19. Calandra, P.; Giordano, C.; Longo, A.; Turco, L. *V. Mater. Chem. Phys.* **2006**, *98*, 494.
20. Tang, J.; Huang, J.; Man, S. *Q. Spectrochim. Acta A* **2013**, *103*, 349.
21. Turkevich, J. *Gold Bull.* **1985**, *18*, 86.
22. Duan, H.; Cui, H.; Zhang, Z.; Liu, B.; Guo, J.; Wang, W. *J. Phys. Chem. C* **2007**, *111*, 4561.
23. Liu, Y.; Male, K. B.; Bouvrette, P.; Luong, J. H. T. *Chem. Mater.* **2003**, *15*, 4172.
24. Wu, H.; Ji, X.; Zhao, L.; Yang, S.; Xie, R.; Yang, W. *Colloids Surf. A* **2012**, *415*, 174.
25. Brust, M.; Walker, M.; Bethell, D.; Schiffrin, D. J.; Whyman, R. *J. Chem. Soc. Chem. Commun.* **1994**, *7*, 801.
26. Newman, J. D. S.; Blanchard, G. J. *Langmuir* **2006**, *22*, 5882.
27. Kumar, A.; Mandal, S.; Selvakannan, P. R.; Pasricha, R.; Mandale, A. B.; Sastry, M. *Langmuir* **2003**, *19*, 6277.
28. Sahiner, N. *Prog. Polym. Sci.* **2013**, *38*, 1329.
29. Yildiz, S.; Aktas, N.; Sahiner, N. *Int. J. Hydrogen Energy* **2014**, *39*, 14690.
30. Yildiz, S.; Sahiner, M.; Sahiner, N. *Eur. Polym. J.* **2015**, *70*, 66.
31. Bengzon-Tan, N. P.; Lee, C. H.; Chen, L.; Ho, K. M.; Lu, Y.; Ballauff, M.; Lei, P. *Polymer* **2015**, *76*, 271.
32. Lu, Y.; Proch, S.; Schrinner, M.; Drechsler, M.; Kempe, R.; Ballauff, M. *J. Matter Chem.* **2009**, *19*, 3955.
33. Wu, S.; Kaiser, J.; Drechsler, M.; Ballauf, M.; Lu, Y. *Colloid Polym. Sci.* **2013**, *291*, 231.
34. Thomas, V.; Namdeo, M.; Mohan, Y. M.; Bajpai, S. K.; Bajpai, M. *J. Macromol. Sci. Pure Appl. Chem.* **2007**, *45*, 107.
35. Sugunan, A.; Thanachayanont, C.; Dutta, J.; Hilborn, J. *G. Sci. Technol. Adv. Mater.* **2005**, *6*, 335.
36. Satarkar, N. S.; Hilt, J. Z. *J. Controlled Release* **2008**, *130*, 246.
37. Wong, J. E.; Gaharwar, A. K.; Müller-Schulet, D.; Dahadur, D.; Richtering, W. J. *Colloid Interface Sci.* **2008**, *324*, 47.
38. Zhang, J.; Xu, S.; Kumacheva, E. *J. Am. Chem. Soc.* **2004**, *126*, 7908.
39. Yousif, A. M. *J. Polym. Res.* **2013**, *20*, 33.
40. Zielinska, A. K.; Sawosz, E.; Grodzik, M.; Chwalibog, A.; Kamaszewski, M. In Annals of Warsaw University of Life Sciences—SGGW, Animal Science; Kaleta, T., Ed.; Warsaw University of Life Sciences Press: Warsaw, **2009**; Vol. *46*, p 249.
41. Sahiner, N.; Yu, H.; Tan, G.; He, J.; John, V. T.; Blake, D. A. *ACS Appl. Mater. Interfaces* **2012**, *4*, 163.
42. Aguilar, J.; Moscoso, F.; Ríos, O.; Ceja, I.; Sánchez, J. C.; Bautista, F.; Puig, J. E.; Fernández, V. V. A. *J. Macromol. Sci. Pure Appl. Chem.* **2014**, *51*, 412.
43. Silva, J. M.; Ortega-Gudiño, P.; Rabelero, M.; Sánchez-Díaz, J. C.; Guerrero-Ramírez, L. G.; Puig, J. E. *J. Macromol. Sci. Pure Appl. Chem.* **2013**, *50*, 596.
44. Song, Y.; Li, Z.; Wang, L.; Yao, Y.; Chen, Ch.; Cui, K. *Microsc. Res. Tech.* **2008**, *71*, 409.
45. Fernandez, V. V. A.; Tepale, N.; Sánchez-Díaz, J. C.; Mendizábal, E.; Puig, J. E.; Soltero, J. F. A. *Colloid Polym. Sci.* **2006**, *284*, 387.
46. Suh, J. S.; Michaelian, K. H. *J. Raman Spectrosc.* **1987**, *18*, 409.
47. Ahern, A. M.; Garrell, R. L. *Langmuir* **1988**, *4*, 1162.
48. Rapp, T. L.; Kowalchyk, W. K.; Davis, K. L.; Todd, E. A.; Liu, K. L.; Morris, M. D. *Anal. Chem.* **1992**, *64*, 2434.
49. Li, C.; Cai, Y.; Zhu, Y.; Ma, M.; Zheng, W.; Zhu, J. *J. Nanopart. Res.* **2013**, *15*, 1922.
50. Zhu, Y.; Qian, Y.; Li, W.; Zhang, M. *Chem. Commun.* **1997**, 1081.
51. Zhu, J. F.; Zhu, Y. J.; Ma, M. G.; Yang, L. X.; Gao, L. *J. Phys. Chem. C* **2007**, *111*, 3920.
52. Zhao, Y.-L.; Chen, Y.; Wang, M.; Liu, Y. *Org. Lett.* **2006**, *8*, 1267.